Imaging hair cell transduction at the speed of sound: Dynamic behavior of mammalian stereocilia

Anders Fridberger*, Igor Tomo, Mats Ulfendahl, and Jacques Boutet de Monvel

Center for Hearing and Communication Research, Departments of Clinical Neuroscience and Otolaryngology, Karolinska Institutet, M1 Karolinska Universitetssjukhuset, SE-171 76 Stockholm, Sweden

Edited by A. James Hudspeth, The Rockefeller University, New York, NY, and approved December 21, 2005 (received for review August 24, 2005)

The cochlea contains two types of sensory cells, the inner and outer hair cells. Sound-evoked deflection of outer hair cell stereocilia leads to fast force production that will enhance auditory sensitivity up to 1,000-fold. In contrast, inner hair cells are thought to have a purely receptive function. Deflection of their stereocilia produces receptor potentials, transmitter release, and action potentials in the auditory nerve. Here, we describe a method for rapid confocal imaging. The method was used to image stereocilia during simultaneous sound stimulation in an *in vitro* preparation of the guinea pig cochlea. We show that inner hair cell stereocilia move because they interact with the fluid surrounding the hair bundles, but stereocilia deflection occurs at a different phase of the stimulus than is generally expected. In outer hair cells, stereocilia deflections were ≈1/3 of the reticular lamina displacement. Smaller deflections were found in inner hair cells. The ratio between stereocilia deflection and reticular lamina displacement is important for auditory function, because it determines the stimulus applied to transduction channels. The low ratio measured here suggests that amplification of hair-bundle movements may be necessary *in vivo* to preserve transduction fidelity at low stimulus levels. In the case of the inner hair cells, this finding would represent a departure from traditional views on their function.

functional imaging | optical flow | cochlear mechanics

The sense of hearing, so critical for communication, depends on a small population of sensory hair cells inside the inner ear. These hair cells come in two versions, the outer and inner hair cells, which have very different functions. Outer hair cells are capable of rapid force generation that serves to amplify the vibration of the hearing organ (1–3). This motor activity leads to a large increase of auditory sensitivity. In contrast, inner hair cells are thought to have a purely sensory role. More than 90% of the afferent fibers of the auditory nerve connect to inner hair cells (4); these are, therefore, absolutely necessary for sound perception. Both cell types have the astounding ability to convert nanometer displacements into electric current. This feat is accomplished by mechanically sensitive ion channels that probably belong to the transient receptor potential family (5). These channels are located along actin-filled protrusions called stereocilia.

Deflection of stereocilia causes channel-gating. The relation between deflection and receptor current has been characterized *in vitro* by pushing stereocilia with glass probes or water jets (e.g., 6–8). However, little information is available from more intact systems. In the cochlea, the stimulus applied to the transduction channels depends on the ratio between stereocilia deflection and sound-evoked vibration of the reticular lamina. The ratio is determined by complicated mechanical processes. In the case of outer hair cells, stereocilia interact with an accessory structure, the tectorial membrane, which couples vibration to the tip of the hair bundles, generating the hair-bundle deflection that triggers force production. Inner hair cells have freestanding stereocilia that lack contact with other structures (9). It is, therefore, unclear how the hair bundles are stimulated. Recordings of receptor potentials from inner hair cells suggest that interactions with the surrounding fluid are important (10–15). Although these recordings provide very valuable data, they are frequently difficult to interpret in terms of stereocilia deflections and, furthermore, show a complex behavior with considerable variation. As a result, the mode of stimulation of inner hair cells has remained unclear. In particular, it is not known how stereocilia deflection is affected by the overlying tectorial membrane, because the precise phase of deflection with respect to the stimulus has never been measured. The lack of direct measurements also means that the stimulus applied to transduction channels in both inner and outer hair cells is poorly defined.

Progress on these issues requires direct determination of stereocilia motion. We accomplished this determination by a special technique for confocal image acquisition. High-resolution images were captured from objects moving at several hundred Hz, something that is impossible with conventional confocal microscopes. Our results are consistent with the idea that inner hair cells are stimulated through interactions with the surrounding fluid. However, hair-bundle deflection occurs at a different phase of the stimulus than is generally expected, perhaps a result of the very narrow space between stereocilia and the tectorial membrane. We also demonstrate that deflections of both inner and outer hair cell stereocilia are quite small. To explain the exquisite sensitivity of the hearing organ, active amplification of hair-bundle movements may be necessary in both inner and outer hair cells.

Results

Time-Resolved Confocal Imaging. To characterize stereocilia motion, it is necessary to examine how different parts of the hair bundle move in relation to surrounding structures. This type of problem may be addressed by imaging techniques such as laser scanning confocal microscopy. However, if a series of confocal images were to be acquired during simultaneous sound stimulation, all information about the motion of the hearing organ would be obscured, because the time required for scanning an image is much longer than the period of the stimulus. Each frame in such a sequence is a mixture of pixels with very different temporal relation to the stimulus.

To deal with this problem, we developed the method for time-resolved confocal imaging shown conceptually in Fig. 1. Fig. 1*A* shows the stimulus waveform. The parts of the waveform highlighted in red correspond to the red pixels in the unprocessed confocal image (Fig. 1*B*). These pixels were all acquired during the same phase of the stimulus. Using custom software, we continuously tracked the temporal relation between each individual pixel and the sound stimulus by sampling the waveform driving the loudspeaker. The confocal microscope's pixel

Conflict of interest statement: No conflicts declared.

This paper was submitted directly (Track II) to the PNAS office.

Freely available online through the PNAS open access option.

Abbreviation: SPL, sound pressure level.

*To whom correspondence should be addressed. E-mail: anders.fridberger@ki.se.

www.pnas.org/cgi/doi/10.1073/pnas.0507231103

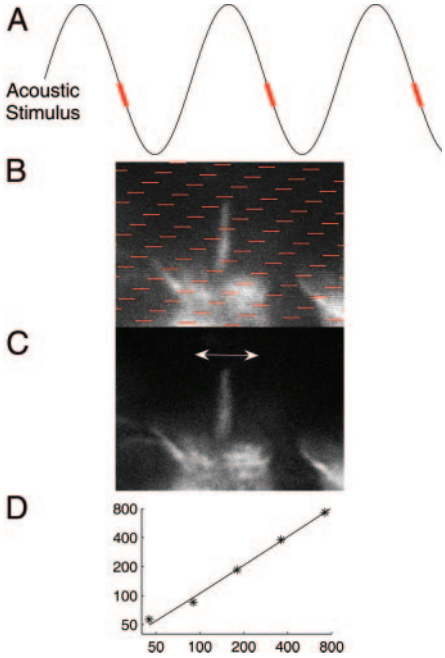

Fig. 1. Method for recovering confocal image sequences from moving inner ear structures. (*A*) The waveform is the acoustic stimulus. (*B*) Image as acquired by confocal microscope. The red parts of the waveform are also shown in *A*. Because scanning of an image proceeds from the top-left to the lower-right corner of the image, same-phase pixels appear in a distinct pattern across the image. (*C*) Same-phase pixels extracted. To generate time-resolved images, pixels with similar phase were grouped to form new images, an example of which is shown in *C*. The arrow shows the direction in which the deflection of the hair bundle occurs, approximately orthogonal to the direction of vibration at the bundle base. In a final processing step, the image sequence was filtered with a three-dimensional Gaussian kernel. This filtered sequence formed the input to the optical-flow-computation algorithm used to quantify motion. (*D*) Linearity. Measured vs. actual motion (nm). The method described above was calibrated against a high-precision piezoelectric translator. The ''true'' motion of a low-contrast test target attached to the translator is given on the figure's *x* axis and the measured motion on the *y* axis. The solid line is defined by the equation $1.01x + 0.004$, confirming a linear relationship between measured and actual motion. Correlation coefficient, 0.996.

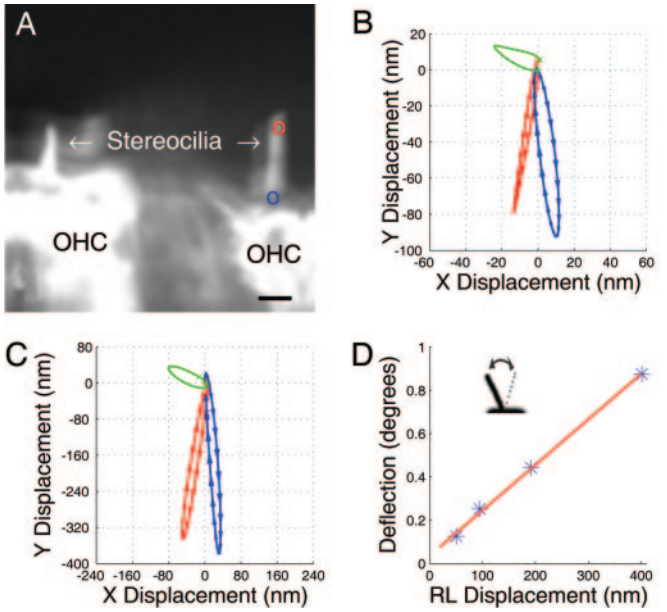

Fig. 2. Outer hair cell motion patterns. (*A*) The confocal image shows two outer hair cells (OHC) during simultaneous sound stimulation at 200 Hz. (Scale bar, 3 μm.) (*B*) The motion of the two points labeled in blue and red in *A* at a stimulus level of 98 dB SPL. The direction of motion is shown by the arrows on each trajectory. The vector difference between the two trajectories, corresponding to the deflection of the hair bundle, is shown in green. (*C*) Data acquired at 110 dB SPL. (*D*) Angular deflection plotted as a function of displacement at the reticular lamina (RL). The angular deflection is the angle formed between the two extremes of the stereocilia deflection. Note that this calculation involves subtraction of trajectories obtained from points at different locations with respect to the center of rotation of the reticular lamina, perhaps resulting in an apparent deflection, even if none is present. However, such a ''geometric'' deflection would have a polarity opposite to that seen here. Calculations showed that this effect was small and would lead to a slight underestimation of the true deflection.

clock triggered each analog-to-digital conversion. Each voltage sample, therefore, corresponds to a pixel at a known position within the image. Complete images were generated by extracting pixels with close to identical phase from a series of images such as the one shown in Fig. 1*B*. This process eliminated motion artifacts (Fig. 1*C*) and allowed the motion of hair cells and stereocilia to be seen.

To quantify motion, a wavelet-based differential optical-flow algorithm was used (see *Methods* and ref. 16). Fig. 1*D* shows a calibration of the method. Over the range 0.045–0.7 μm, the measured motion closely approximated the actual motion of a fluorescent target attached to a high-precision piezoelectric translator. This range of displacements corresponds to those encountered during actual experiments. The amplitudes of reticular lamina vibration described below are similar to those found in living anesthetized guinea pigs at ≈70 dB sound pressure level (SPL) (17), ≈150 nm.

Hair-Bundle Displacements. Fig. 2*A* shows two outer hair cells from the apical, low frequency region of the cochlea. Sound stimulation caused motion of both hair cells and their hair bundles. The hair bundles appeared as stiff rods, pivoting around their points of attachment to the hair cell.

These motions were quantified by using the optical-flow algorithm. The blue circle in Fig. 2*A* marks a location on the reticular lamina where stereocilia attach to the hair cell. As seen in the blue trajectory in Fig. 2*B*, motion at this point almost coincided with the long axis of the stereocilium. Studies have shown that vibration amplitudes at the reticular lamina are similar to those of the basilar membrane in this type of preparation (18). The red circle in Fig. 2*A* marks the tip of the stereocilium, which moved in a direction different from that of the base (compare the red and the blue trajectories in Fig. 2*B*). This difference produced hair-bundle deflection, the size of which was obtained by finding the difference between the two trajectories. The computed deflection is shown in green. As the hair cells moved down toward the scala tympani, the bundle deflected to the left, reaching a maximum of 28 nm (Fig. 2*B*). Peak bundle deflection coincided with peak displacement of the reticular lamina, downward displacement of the organ of Corti resulting in deflection in the inhibitory direction. The movement of the other hair cell in this image was similar (data not shown).

None of the three trajectories in Fig. 2*B* returned exactly to the origin. The distance between the last point on the trajectory and the origin may be regarded a measure of the cumulative error of the optical-flow calculation. The blue trajectory ended ≈1 nm from the origin, whereas the red trajectory showed a 5-nm discrepancy. These values correspond to a total error in the range 1–6%. A conservative estimate is, therefore, that the error in the trajectory showing the deflection is <12%.

When the stimulus level increased 12 dB, a 12-dB increase in hair-bundle deflection was seen (Fig. 2*C*). Thus, deflection of outer hair cell stereocilia is a linear function of reticular lamina

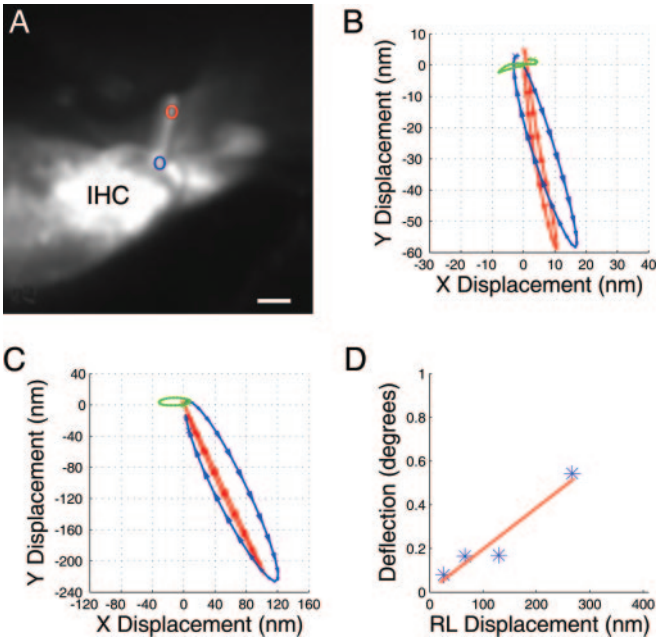

Fig. 3. Inner hair cell motion patterns. (*A*) Confocal image. (*B*) As in Fig. 2, the motion of the red and blue point in *A* at a stimulus level of 98 dB SPL. The difference between these points is given by the green trajectory. (*C*) Data acquired at 110 dB SPL. (*D*) Angular deflection as a function of reticular lamina (RL) displacement. IHC, inner hair cell. (Scale bar, 3 μm.)

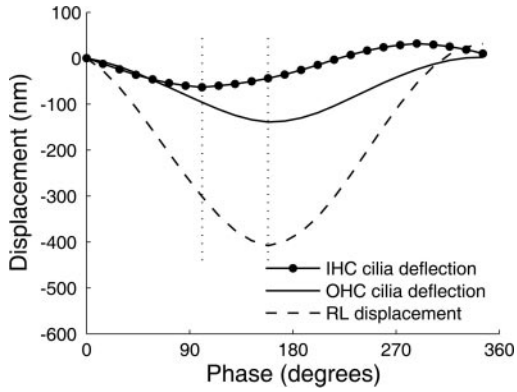

Fig. 4. Relation between stereocilia deflection and displacement of the reticular lamina (RL). Both cells were from the same position along the cochlear spiral. IHC, inner hair cell; OHC, outer hair cell. Phase 0 corresponds to the first image in the series. Stimulus level was 104 dB SPL. Negative-going RL displacement denotes motion toward scala tympani. Note the phase difference between inner and outer hair cells. The left dotted vertical line was drawn through the negative peak of the inner hair cell stereocilia deflection; the right dotted line through the negative peak of the outer hair cell bundle deflection.

displacement under these experimental conditions. The only important qualitative difference was that motion components directed along the figure's x axis seemed less pronounced at higher intensity. Therefore, trajectories appeared less elliptical. These data may also be expressed as the angular deflection. Angular deflections were obtained by computing the arctangent of the ratio between stereocilia deflection and the length of the hair bundle (see also Fig. 2*D Inset*). As shown in Fig. 2*D*, angular deflections ranged between 0.13° and 0.88° for the four stimulus levels used here. The relation between angular deflection and the displacement of the reticular lamina was approximated by a straight line with a slope of 0.21°/100 nm.

Images were also acquired from inner hair cells. The cell shown in Fig. 3*A* came from the same preparation as the cells in Fig. 2, the position along the cochlear spiral was the same, stimulus levels were identical, and data may, therefore, be compared directly. The trajectories show some clear differences from the ones recorded from outer hair cells. First, the overall direction of motion was nearly the same at the top and at the base of the hair bundle. Deflection arose largely because the base of the stereocilium showed more pronounced elliptical motion than did the tip. Second, at all stimulus levels, this inner hair cell showed smaller displacements than outer hair cells. In Fig. 3*B*, the peak-to-peak deflection was 14 nm, as compared with 28 nm for the outer hair cell. These differences remained as the stimulus intensity increased. However, the comparison may be influenced by slight differences in the apparent length of the hair bundle. Angular deflection is, therefore, a more reliable measure; angular deflection ranged from 0.08° to 0.54°, or ≈61% of the value found for the outer hair cells (see Figs. 2*D* and 3*D*). The line has a slope of 0.19°/100 nm.

Following acquisition of these data, we applied the lectin Con A, tagged with the green-fluorescent marker Alexa Fluor 488. This compound labeled the tectorial membrane, allowing us to verify that the membrane was intact and appeared in the expected position (data not shown). The tips of outer hair cell stereocilia appeared to be embedded in the tectorial membrane, but this was not the case for the inner hair cell (see also Fig. 6).

Close examination of the trajectories in Fig. 3 *B* and *C* reveal that downward displacement of the reticular lamina resulted in hair-bundle deflection to the left, which is the inhibitory direction. Because of the apparent lack of contact between inner hair cell stereocilia and the tectorial membrane, interaction with the fluid surrounding the hair bundle is a possible explanation for the deflection (see *Discussion*). At frequencies used here, such interaction is expected to depend on the rate of displacement of the reticular lamina. Because outer hair cells respond to the displacement of the hearing organ, a phase difference is predicted between inner and outer hair cell stereocilia deflection.

Fig. 4 shows hair-bundle deflections plotted together with the displacement at the reticular lamina. As expected, maximum deflection of outer hair cell stereocilia coincided with peak displacement of the reticular lamina. This was not the case for the inner hair cell. Maximum deflection occurred before the reticular lamina had reached its peak displacement. Fourier transformation showed that inner hair cell stereocilia deflection led reticular lamina displacement by 53°.

Response amplitudes and phases vary according to position along the cochlear spiral, so adequate comparison of inner and outer hair cell cilia vibration requires that the cells are located at the same position. In 25 cell pairs from four different preparations, where each pair was located at the same position within the cochlear spiral, the mean phase lead for the inner hair cell bundle deflection was 44° (95% confidence interval 25–62°).

This phase difference could arise if different parts of the reticular lamina, where stereocilia are attached, vibrate with a different phase. However, analysis of the data showed that the base of stereocilia on inner and outer hair cells moved with close to identical phase (average phase difference, 5°).

Response Amplitudes. Fig. 5 shows data from the same 25 cell pairs mentioned above. In all cases, angular deflections were larger in outer hair cell stereocilia. This difference was statistically significant ($P < 0.00001$ by Student's t test for paired variables). Fig. 5*B* plots angular deflection as a function of reticular lamina displacement for 41 inner and 106 outer hair cells from 10 different preparations. In this figure, inner hair-cell-bundle deflections are plotted against displacement measured at the

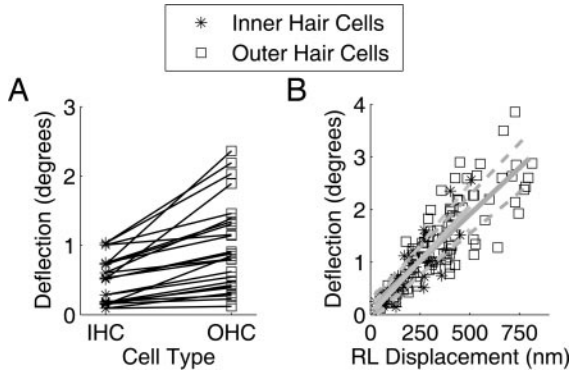

Fig. 5. Hair bundle deflections. (*A*) Angular deflection of 25 pairs of inner and outer hair cells, each located at close to identical position along the basilar membrane's length. Anatomically, outer hair cells outnumber inner hair cells, so there are more outer hair cell points in this graph. Symbols apply to *A* and *B*. (*B*) Angular deflection as a function of reticular lamina (RL) displacement in all hair cells, regardless of their relative location. The solid lines were drawn by linear regression and had a slope of 0.35°/100 nm for outer hair cells and 0.41°/100 nm for inner hair cells (correlation coefficients of 0.85 and 0.86, respectively). Thin dashed lines show fit ± 1 SD. The mean stereocilia length in inner hair cells was 5.1 μm and in outer hair cells 5 μm.

base of the inner hair cells' bundle. Outer hair cell angular deflections are plotted against displacement at their bundle bases. The slopes of the regression lines were not significantly different ($P = 0.52$ by Fisher's test). Thus, although inner hair cells show smaller absolute deflections, the "transformer ratio" from reticular lamina motion to stereocilia deflection was the same as in outer hair cells. These data were acquired from cells in different positions within the apical turn, perhaps explaining some of the apparent scatter.

From Figs. 2–5, it is apparent that stereocilia deflections are much smaller than the displacement of the reticular lamina. On average, the ratio between outer hair cell stereocilia deflection and reticular lamina displacement was 0.35 ± 0.12 (mean ± SD). For inner hair cells, the corresponding ratio was 0.37 ± 0.13 (the displacement of the reticular lamina was smaller near inner hair cells, making the ratio similar to the outer hair cell value despite the smaller deflections of inner hair cell stereocilia).

Contribution from the Active Process. At low and moderate stimulus levels, force generated by outer hair cells will boost vibration. To assess a possible contribution from such active processes, inner hair cells were imaged before and after application of the transduction channel blocker streptomycin. By blocking transduction channels, amplification based on stereocilia and somatic motility were prevented from influencing the response of the preparation.

Streptomycin, at 100 μM, caused no consistent change in organ of Corti vibrations. Minor increases (<3 dB) at the reticular lamina were seen in five of nine preparations. Minor decreases or a lack of change was seen in four of nine preparations. Hair-bundle deflections changed their amplitude in proportion to the change measured at the reticular lamina, but the phase of the deflection was unaltered in eight of nine preparations, demonstrating that the active process made no significant contribution to sound-evoked responses at these stimulus levels in this type of preparation.

Discussion

In this study, an imaging technique was designed and used to image stereocilia displacements during sound stimulation at a frequency that was appropriate for the cochlear location studied. Calibrations showed that motion was accurately measured over the interval from 0.045 to 0.7 μm. These limits are not intrinsic to the technique. By increasing the pixel size, larger displacements may be measured with similar accuracy. Hardware limitations prevented the use of pixel sizes <110 nm; future versions of the microscope may, therefore, permit measurements at even lower sound pressures. This type of acquisition system may be used in any system where stimulus and response are periodic.

For sound perception to be possible, vibration of the hearing organ must be transformed into stereocilia deflection. The ratio between stereocilia deflection and reticular lamina motion is important for cochlear function, because it determines the stimulus applied to transduction channels. We measured a ratio of 0.35 ± 0.12 in outer hair cells. The only previous measurement of hair-bundle deflection *in situ* was obtained with very-low-frequency artificial stimulation in a bisected cochlea preparation (19) (ratio of 0.7–1.1). It is, perhaps, not surprising that the ratios differ, given the dissimilar modes of stimulation.

Our streptomycin experiments show that the amplifying mechanisms inherent to the outer hair cells do not function to the extent seen in a living animal under the experimental conditions used here. Frequency tuning may, therefore, be less sharp and response amplitudes lower than is the case *in vivo*. Previous studies, and data obtained with the current technique, showed that mechanical frequency-tuning curves obtained in this preparation (20) are similar to inner hair cell receptor-potential tuning curves measured from the same cochlear region *in vivo* at 50–70 dB SPL (21). At these stimulus levels, the response of the hearing organ begins to be dominated by passive mechanics. To understand cochlear function, it is useful to start by defining the response of such a passive system, because passive mechanics underlie organ of Corti vibrations at all stimulus levels *in vivo*.

In vivo, with a fully functioning cochlear amplifier, displacements of the basilar membrane are in the range 0.1–1 nm near the threshold of hearing (22). If the above ratio applied also in this situation, stereocilia deflections would be in the range 0.035–0.35 nm. These values appear quite small. For comparison, it is noted that the Brownian motion of hair bundles is on the order of 1–3 nm (23), although this comparison has limited applicability because a hair bundle driven by a weak sound stimulus is not in thermodynamic equilibrium with its surroundings. In hair cells studied *in vitro*, the minimum stereocilia deflection that can reliably be detected in the cell's receptor current is 2–5 nm (24). A main function of the cochlear amplifier may, therefore, be to increase the ratio between stereocilia deflection and organ displacement.

How does the reasoning in the previous paragraph apply to the inner hair cells? We show here that inner hair cell stereocilia deflections are even smaller than those found in outer hair cells. One possibility is that the molecular motors of the outer hair cells selectively amplify the fluid flow in the space underlying the tectorial membrane (25). In addition, hair cells of both mammals and lower vertebrates are endowed with stereociliary amplifiers (2, 3, 26), a mechanism that may be most effective when overlying accessory structures are removed, a condition that is fulfilled naturally in inner hair cells. In such a case, the inner hair cell would boost its own stereocilia vibration, thereby increasing transduction fidelity at low stimulus levels. The traditional view is that inner hair cells respond passively to fluid flow around the hair bundle, which is generated through the shearing motion of the reticular lamina and the overlying tectorial membrane. Either of the above cases, therefore, represents a departure from traditional views on inner hair cell function.

How is deflection of inner hair cell stereocilia generated? This is a crucial question, because inner hair cells provide the sole input to >90% of the afferent fibers of the auditory nerve. Because of an apparent lack of contact with surrounding structures, interaction between stereocilia and the surrounding fluid is thought to be important (10). Assuming that the influence of

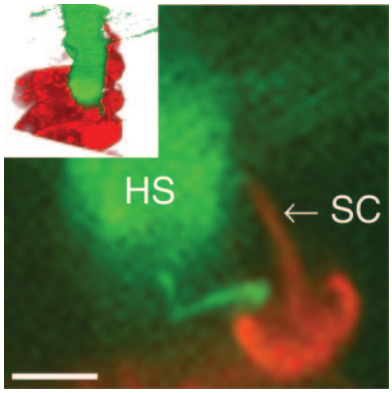

Fig. 6. Confocal micrograph showing an inner hair cell labeled with RH795 (red) and a part of the tectorial membrane (green; soy bean agglutinin/Alexa Fluor 488). The plane of the section was oblique; the length of the stereocilia (SC) is, therefore, somewhat exaggerated. Note the close proximity of the hair bundle and Hensen's stripe (HS) and the small strands of tissue connecting the cell body of the inner hair cell with the tectorial membrane. These characteristics are also apparent in the three-dimensional reconstruction (*Inset*). (Scale bar, 5 μm.)

the tectorial membrane is negligible, fluid interaction at low stimulus frequencies is expected to depend on the velocity of the organ of Corti rather than its displacement, so a 90° phase difference would ensue between inner hair cell stereocilia deflection and the displacement of the hearing organ. Early receptor potential recordings from the cochlear apex supported this theory by showing a phase difference close to 90° at 200 Hz (14), but more recent work generally showed a value of 45° (27) and that some inner hair cells appeared to be driven by displacement alone, even at these stimulus frequencies (e.g., figures 3 and 4 in ref. 28; ≈18° at 50 dB SPL and 140 Hz). However, receptor potentials are affected by the low-pass filter formed by the cell membrane and, possibly, by activation of ion channels other than the mechanically sensitive ones. Microelectrodes may also damage sensory cells and impede organ vibration (29). Therefore, it is frequently difficult to interpret electrophysiological recordings in terms of stereocilia deflections. Our inner hair cell stereocilia deflections had a 44° phase lead over the displacement of the reticular lamina. This phase value means that apical turn inner hair cells respond to a combination of velocity and displacement at the frequency used here, which is close to the best frequency. It would appear that there is a complex interaction among stereocilia, the surrounding fluid (30), and structures around the hair bundle (31). Inner hair cell stereocilia are closely apposed to the part of the tectorial membrane called Hensen's stripe (Fig. 6). Such structural relations may affect fluid flow around stereocilia (32, 33), leading to nontrivial phase relations such as the one that we found.

In summary, this study describes direct measurements of a crucial step in sound perception, the deflection of stereocilia on inner and outer hair cells. Our data show that stereocilia deflections are smaller in inner than in outer hair cells, that apical turn inner hair cells respond to a combination of displacement and velocity near their best frequency, and that outer hair cell stereocilia deflect by ≈1/3 of the displacement of the hearing organ.

Methods

Preparation and Sound Stimulation. The preparation was described in detail in ref. 34. By using procedures approved by the local ethics committee (permit 311/03), guinea pigs were decapitated and the temporal bone attached to a holder, with the external auditory meatus facing a loudspeaker. A part of the bone covering the apical turn of the cochlea was removed, the preparation being immersed in an endolymph-like solution containing 150 mM KCl, 5 mM NaCl, 3 mM glucose, 0.03 mM $CaCl_2$, 25 mM Hepes, 2 mM K_2PO_4, and albumin (5 g/liter). Scala tympani were perfused with a perilymph-like solution (Minimum Essential Medium, Invitrogen) that also contained 4 μg/ml of calcein acetoxymethyl ester (Molecular Probes). This dye stained Reissner's membrane, allowing its visualization with regular fluorescence microscopy. After dye loading, Reissner's membrane was ruptured by using a fine needle. The opening thus created caused the fluid in scala media to gradually equilibrate with the medium surrounding the preparation. Because the preparation was immersed in an endolymph-like solution, the ionic milieu in scala media closely approximated normal conditions. The continuous scala tympani perfusion retained the normal ionic composition in this compartment.

The dye RH795 was thereafter added to the perfusion medium (12.5 μg/ml; Molecular Probes). Because of the opening in Reissner's membrane, this dye stained stereocilia on both inner and outer hair cells. To ensure that the organ of Corti was intact, the preparation was visualized with a low-power lens. If the structure appeared disturbed or the sensory cells showed swelling or other abnormalities, the preparation was discarded. A Zeiss LSM510 laser scanning confocal microscope with a ×40, NA 0.8 water-immersion lens was subsequently used for visualization at a pixel size of 110 nm. For anatomical reasons, a perfect cross-section of the organ of Corti cannot be obtained without physical sectioning. However, by tilting the preparation with respect to the optical axis of the microscope, images close to true cross-sections were obtained. The angle of the preparation with respect to the optical axis of the microscope was assessed by acquiring a stack of 20 confocal images separated by 0.8–2 μm along the z axis. The angle was directly determined from the reconstructed pixel volume. In Figs. 2 and 3, which typify our data, the preparation was 18° off from a true cross-section. Because the major axis of vibration is in the plane of a cross-section, this slight angle would, at most, cause a 5% change of vibration amplitudes. The data shown were not corrected for this effect.

Sound stimulation was at 200 Hz. Tuning curves acquired with the present technique show that best frequencies of this cochlear location ranges between 150 and 225 Hz. Stimulus levels were between 88 and 110 dB re 20 μPa. Because of immersion and the opening of the apical turn, the effective stimulus level is reduced by as much as 20–30 dB (35). Values given in the text were not corrected for this attenuation.

Time-Resolved Confocal Imaging. The signal driving the loudspeaker was sampled with a National Instruments PCI-6115 analog-to-digital converter. Each conversion was triggered by the microscope's pixel clock. To verify synchronization, a light-emitting diode was placed on the stage of the microscope. The diode was driven by square waves from a function generator, positive voltage resulting in light emission. By imaging the diode, we verified that negative-to-positive voltage transitions corresponded to bright pixels in the image (and the inverse).

The arrangement described above results in an array of sampled voltages. Voltages in this array may be used as phase values, provided that the derivative is also computed (samples with positive derivative and positive voltage correspond to phase 0–89° of the stimulus waveform, samples with positive voltage and negative derivative to phase 91–180°, etc.). After finding locations in the array with similar voltage and derivative, corresponding pixels were extracted from the stack of confocal images. These pixels were projected onto a single plane, forming a "resampled" image, where all pixels were acquired at the same phase of the stimulus. The process was repeated for different voltages and derivatives until a full cycle had been recovered.

This procedure eliminated motion artifacts (Fig. 1*C*) and allowed the motion of hair cells and stereocilia to be seen.

Analysis of Hair-Bundle Motion. In a first step, the image sequence was normalized by setting the mean intensity of each frame to a constant value, equal to the mean intensity of the first frame to correct for the slow fading of intensity that sometimes occurred during acquisition. Thereafter, same-phase pixels were extracted by using the techniques described above. This resampling produced an image sequence containing one cycle of the hair cell's motion. The resampled image sequence was smoothed by convolution with a three-dimensional Gaussian filter by using circular averaging along the time axis, amounting to imposing a periodicity constraint on the image sequence, which was important to take better advantage of the periodic nature of the hair bundles' trajectories. Note that, although the motion of the organ of Corti in response to a pure tone can be assumed to be periodic on average, deviations from periodicity (because of noise or other factors) might occur from one cycle to another. Such deviations are expected to be small and would have been lost in the resampling step. This analysis was designed to extract only the periodic component of the hair bundle's motion. In the final step, the normalized, resampled, and smoothed image sequence was fed to the optical-flow algorithm. The computed hair-bundle displacements were then further analyzed, as described in *Results*. Compared with our earlier studies (16, 18), the time-circular averaging and much smaller pixel size resulted in a significant increase in sensitivity.

In the text above, the displacement of the reticular lamina refers to the Euclidean vector magnitude measured at the base of the hair bundle, thus reflecting motion components along both axes of the image.

Calibration. To verify system performance, fluorescent paper fibers were glued to a piezoelectric translator (model P841-10, Physik Instrumente, Waldbronn, Germany) and imaged with the same objective lens, pixel size, scan speed, and stimulus frequency as those used during actual experiments. The translator had an integrated position sensor and an active feedback system with 1-kHz bandwidth, allowing the exact displacement of the low-contrast target to be monitored and ensuring that the translator's motion closely followed the applied command signal.

Streptomycin. In a separate series of experiments, the transduction channel blocker streptomycin was applied to the preparation (final concentration, 100 μM; Sigma). After an initial set of image sequences had been acquired, this substance was added to both the perfusion medium and to the fluid surrounding the preparation. Ten minutes later, several new sets of images were acquired.

We thank Åke Flock (Karolinska Institutet) for the gift of indispensable equipment and Jun Hyodo and Alessandro Marin for help with acquiring the images shown in Fig. 6. This work was supported by the Swedish Research Council, the Human Frontier Science program, Hörselskadades Riksförbund, the Tysta Skolan Foundation, the Åke Wiberg Foundation, the Tore Nilson Foundation, the Swedish Society of Medicine, the Petrus and Augusta Hedlund Foundation, and Karolinska Institutet.

1. Brownell, W. E., Bader, C. R., Bertrand, D. & de Ribaupierre Y. (1985) *Science* **227,** 194–196.
2. Chan, D. K. & Hudspeth, A. J. (2005) *Nat. Neurosci.* **8,** 149–155.
3. Kennedy, H. J., Crawford, A. C. & Fettiplace, R. (2005) *Nature* **433,** 880–883.
4. Spoendlin, H. (1969) *Acta Otolaryngol.* **67,** 239–254.
5. Corey, D. P., Garcia-Anoveros, J., Holt, J. R., Kwan, K. Y., Lin, S. Y., Vollrath, M. A., Amalfitano, A., Cheung, E. L., Derfler, B. H., Duggan, A., *et al.* (2004) *Nature* **432,** 723–730.
6. Howard, J. & Hudspeth, A. J. (1988) *Neuron* **1,** 189–199.
7. Kros, C. J., Lennan, G. W. T. & Richardson, G. P. (1995) in *Active Hearing*, eds. Flock, Å., Ottosson, D. & Ulfendahl, M. (Elsevier, Oxford, U.K.), pp. 113–125.
8. Kennedy, H. J., Crawford, A. C. & Fettiplace, R. (2003) *Nat. Neurosci.* **6**, 832–36.
9. Lim, D. J. (1986) *Hearing Res.* **22,** 117–146.
10. Dallos, P., Billone, M. C., Durrant, J. D., Wang, C.-Y. & Raynor, S. (1972) *Science* **177,** 356–358.
11. Nuttall, A. L., Brown, M. C., Masta, R. I. & Lawrence, M. (1981) *Brain Res.* **211,** 171–174.
12. Patuzzi, R. B. & Yates, G. K. (1987) *Hearing Res.* **30,** 83–98.
13. Russell, I. J. & Sellick, P. M. (1983) *J. Physiol.* **338,** 179–206.
14. Dallos, P. (1985) *J. Neurosci.* **5,** 1591–1608.
15. Wada, H., Takeda, A. & Kawase, T. (2002) *Hearing Res.* **165,** 165–176.
16. Fridberger, A., Widengren, J. & Boutet de Monvel, J. (2004) *Biophys. J.* **86,** 535–543.
17. Zinn, C., Maier, H., Zenner, H. & Gummer, A. W. (2000) *Hearing Res.* **142,** 159–183.
18. Fridberger, A. & Boutet de Monvel, J. (2003) *Nat. Neurosci.* **6,** 446–448.
19. Hu, X., Evans, B. N. & Dallos, P. (1999) *J. Neurophysiol.* **82,** 2798–2807.
20. Ulfendahl, M., Khanna, S. M., Fridberger, A., Flock, Å., Flock, B. & Jäger, W. (1996) *J. Neurophysiol.* **76,** 3850–3862.
21. Dallos, P. (1986) *Hearing Res.* **22,** 185–198.
22. Robles, L. & Ruggero, M. A. (2001) *Physiol. Rev.* **81,** 1305–1352.
23. Jaramillo, F. & Wiesenfeld, K. (1998) *Nat. Neurosci.* **1,** 384–388.
24. van Netten, S. M., Dinklo, T., Marcotti, W. & Kros, C. J. (2003) *Proc. Natl. Acad. Sci. USA* **100,** 15510–15515.
25. Gummer, A. W., Nowotny, M., Scherer, M. P. & Vetešník, A. (2005) in *Auditory Mechanisms: Processes and Models*, eds. Nuttall, A. L., Ren, T., Gillespie, P. G. & Walker, R. (World Scientific, Singapore), in press.
26. Martin, P. & Hudspeth, A. J. (1999) *Proc. Natl. Acad. Sci. USA* **96,** 14306–14311.
27. Cheatham, M. A. & Dallos, P. (1999) *J. Acoust. Soc. Am.* **105,** 799–810.
28. Cheatham, M. A. & Dallos, P. (1998) *J. Acoust. Soc. Am.* **104,** 356–369.
29. Ruggero, M. A., Narayan, S. S., Temchin, A. N. & Recio, A. (2000) *Proc. Natl. Acad. Sci. USA* **97,** 11744–11750.
30. Aranyosi, A. J. & Freeman, D. M. (2004) *Biophys. J.* **87,** 3536–3546.
31. Legan, P. K., Lukashkina, V. A., Goodyear, R. J., Lukashkin, A. N., Verhoeven, K., Van Camp, G., Russell, I. J. & Richardson, G. P. (2005) *Nat. Neurosci.* **8,** 1035–1042.
32. Billone, M. & Raynor, S. (1973) *J. Acoust. Soc. Am.* **54,** 1143–1156.
33. Steele, C. R. & Puria, S. (2005) *Int. J. Solids Structures* **42,** 5887–5904.
34. Fridberger, A., Boutet de Monvel, J. & Ulfendahl M. (2002) *J. Neurosci.* **22,** 9850–9857.
35. Franke, R., Dancer, A., Khanna, S. M. & Ulfendahl, M. (1992) *Acustica* **76,** 173–182.